Density Functional Theory Calculation and X-ray Absorption Spectroscopy Studies of Structure of Vanadium-Containing Aluminophosphate VAPO-5

H. Y. Cheng,* E. Yang, and C. J. Lai

Department of Chemistry, Tunghai University, Taichung, Taiwan

K. J. Chao,* A. C. Wei, and J. F. Lee†

Department of Chemistry, National Tsinghua University, Hsinchu, Taiwan

Received: November 10, 1999

Theoretical calculation using density functional B3LYP correlation-exchange is employed to study the structure of different sizes of the VAPO-5 clusters. The results indicate that the substitution of either the phosphorus site or the aluminum site of the aluminophosphate-5 framework with vanadium is generally not feasible. The calculated structures are comparable with those from the in-situ X-ray absorption (XANES and EXAFS) of the V K-edge. The isolated vanadium was found to exist as a mono-oxo $(V^{4+}=O)(O_t)_4$ species for reduced, dehydrated VAPO-5 and as a di-oxo $V^{5+}O_4$ species for calcined, dehydrated VAPO-5. The coordination geometry of the mono-oxo V^{4+} species is sensitive to the presence of water molecules, and the water molecules may exchange with the framework oxygens that are coordinated to the V^{4+} center.

Introduction

Transition-metal incorporated molecular sieves are known to possess unique catalytic properties in hydrocarbon conversions. Such properties are thought to be derived from the framework geometry, acid properties of the molecular sieve, and redox behaviors of the framework-bound transition-metal ions. The vanadium-containing aluminophosphate-5 molecular sieve (VAPO-5) was found to be an active catalyst for the selective oxidation of alkanes and cycloalkanes, by oxygen in the gas phase,[1] and the alkene epoxidation, as well as the benzylic oxidation, by peroxide in liquid phase.[2] Because these catalytic properties are from the isolated vanadium ions in the aluminophosphate-5 framework (AFI), the characterization of both the local structure and the oxidation state of vanadium ions in VAPO-5 after synthesis and under redox conditions is important.

Electron spin resonance (EPR) and ^{51}V NMR studies[2−6] suggested that at low concentration, vanadium exists mainly as well-dispersed and immobilized monomeric vanadyl(IV) species in as-synthesized VAPO-5, and upon calcination, the vanadium(IV) species could be oxidized to vanadium(V). From the elemental composition and the finding of the existence of the mineral of $2Al_2O_3{\cdot}V_2O_5{\cdot}P_2O_5{\cdot}16H_2O$ and vanadyl(V) phosphate, Jhung et al.[3] and Montes et al.[4] proposed that vanadium(IV) substitutes for phosphorus(V) in AFI, whereas Rigutto et al.[2] suggested that vanadium occupies aluminum sites, rather than phosphorus sites. By combining EPR with electron spin−echo modulation (ESEM) studies, Prakash et al.[6] supported the notion that vanadium ions could be at sites nearer to the framework aluminum than to the phosphorus. According to EPR and diffuse reflectance spectroscopy (DRS) measurements, Weckhuysen et al.[7] claimed that the V^{4+} species are in a pseudo-octahedral coordination state, rather than being tetrahedral for a true isomorphous substitution in AFI lattice. By IR measurements, Lohse et al.[8] further pointed out that VO^{2+} ions are bound to the inner surface of the AFI framework through condensation with hydroxyl groups. Because the characteristic EPR features of a tetrahedral V^{4+} were not observed, even down to liquid-helium temperature, Lohse[8] also suggested that vanadium(IV) is not capable of occupying a regular tetrahedral site in the AFI framework, which was confirmed by UV−vis spectroscopic investigations.[5,7] Because EPR is a sensitive tool for the paramagnetic V^{4+} of d^1 species but ineffective for the diamagnetic V^{5+} of d^0 species, most of the EPR studies were focused on as-synthesized VAPO-5 and the change in oxidation state of the vanadium species during calcination. Low vanadium-containing VAPO-5 EPR studies reach the same conclusion as above, that the highly dispersed VO^{2+} ion of as-synthesized VAPO-5 is in a distorted octahedral or a square pyramidal coordination environment, rather than in a tetrahedral coordination. VO^{2+} is expected to at least bond to either a framework aluminum or a phosphorus site.

Recent ESEM studies coupled with EPR measurements[6], X-ray absorption (XAS) studies (including preedge and near-edge spectroscopy (XANES)), and extended fine structure analysis (EXAFS)[9] described as-synthesized and reduced VAPO-5 of V^{4+} ions as isolated monomeric VO^{2+} complex units coordinated to two framework oxygens with or without either three water molecules or one hydroxyl group and two water molecules. Upon dehydration, the coordination symmetry of V^{5+} was found to shift gradually from either square pyramidal or octahedral to tetrahedral; an isolated tetrahedral V^{5+} species was proposed to be the active site for the oxydehydrogenation of propane reaction.[10] Furthermore, if oxidation reactions with electron transfer are catalyzed by metal-incorporated aluminophosphate, aluminosilicate, and silicate molecular sieves, they most likely will involve ligand exchange and reactant-metal interaction, accompanied perhaps by a reversible change in coordination state.[11] Both V^{4+} and V^{5+} ions would be expected to coordinate to water molecules very effectively if water is present. This illustrates the critical need for in-situ measurements

† Synchrotron Radiation Research Center, Hsinchu,Taiwan.

10.1021/jp993981e CCC: $19.00
Published on Web 03/31/2000

that are sensitive to metal ions in both oxidized and reduced forms. The results from such measurements can not only establish the local structure of the transition-metal ion in metal-contained molecular sieves, e.g., V^{4+} and V^{5+} ions in VAPO-5, but also clarify the misconception that results from pretreatments and postreaction. This in-situ characterization can provide correct information about the nature of catalytically active sites.

In this study, the in-situ XAS technique is used to probe the local environment of vanadium sites in VAPO-5 before and during redox treatment and the effect of the presence of water molecules. Assuming that the EXAFS is focused on first-shell atoms around a central V ion, the location of V in the aluminophosphate framework is thus studied by cluster modeling and quantum chemical calculation, based on density functional theory. Full and constrained geometry optimizations have been performed to obtain calculated geometries, which are then compared with in-situ EXAFS results. The results can predict the possible position of the anchored vanadium species in the AFI framework.

Experimental Section

Sample Preparation. VAPO-5 was synthesized under hydrothermal condition with water from the reactant mixture of orthophosphoric acid (85%, Merck), aluminum source (Versal 150), tripropylamine (Merck), and vanadyl sulfate ($VOSO_4 \cdot 5H_2O$, Fluka). The reactant gel was prepared according to the following steps: To 20.5 g of deionized water was slowly added 5.14 g of aluminum source under vigorous stirring. Next, the orthophoric acid solution (12.23 g of H_3PO_4 + 10 g of deionized water) was added rapidly, and the resulting solution was stirred for 30 min. Subsequently, the $VOSO_4$ solution (1.35 g of $VOSO_4$ + 15 g of deionized water) was added dropwise to the above mixture, which was then stirred for an additional 20 min. Finally, 10 mL of tripropylamine was added dropwise. The final mixture, with a molar ratio of 1.0:0.95:0.1:1.4:50 ($P_2O_5/Al_2O_3/VO/Pr_3N/H_2O$), was stirred for another 20 min and was then transferred into a Teflon-lined stainless steel autoclave, in which it was kept at 170 °C for 1 d in a pretreated oven. After crystallization, the greenish crystals were washed with distilled water and were dried at 70 °C. To remove the organic template molecules encapsulated in the as-synthesized VAPO-5, it was heated to 500 °C at a heating rate of 1 °C/min, and it was kept at 500 °C for the first 4 h under a flow of dry air and then for another 4 h under a flow of dry O_2. The as-synthesized and calcined samples were examined by XRD on a powder diffractometer (Rigaku DMAX II) with Cu Kα radiation. The content of vanadium in VAPO-5 was 1.8 wt %, which was determined by inductively coupled plasma-atomic emission spectroscopy (ICP-AES).

X-ray Absorption Spectroscopy (XAS). XAS measurements were performed on the beamline BL17C at the Synchrotron Radiation Research Center (SRRC) in Taiwan, with a storage ring energy of 1.5 GeV and a beam current between 120 and 200 mA.

Prior to the XAS measurements, the yellow, calcined hydrated VAPO-5 was mixed with boron nitride powder (Merck) at a predetermined ratio, the mixture was mounted in an in-situ cell,[12−14] and the XAS data of calcined, hydrated VAPO-5 was collected under ambient condition. Subsequently, the in-situ cell was heated from room temperature to 200 °C at a heating rate of 6 °C/min, and it was maintained at 200 °C for 1 h under the flow of He to remove the adsorbed water on the sample. The in-situ cell was then cooled to room temperature, and the XAS spectrum of the calcined, dehydrated VAPO-5 was measured under the He flow. The calcined, dehydrated sample was heated again from room temperature to 500 °C at a heating rate of 6 °C/min, and it was maintained at 500 °C for 1 h under the flow of H_2 to give a gray, reduced, and dehydrated VAPO-5 sample, which was then cooled to room temperature under H_2 flow. The XAS data were collected under He flow. Finally, the reduced, dehydrated sample was purged with He and heated from room temperature to 500 °C at a heating rate of 6 °C/min, and it was maintained at 500 °C for 1 h under the flow of O_2/He (1:9) and then cooled to room temperature to give a yellow and reoxidized VAPO-5. In addition, the calcined, hydrated VAPO-5 was heated to 500 °C at a heating rate of 6 °C/min, at which it was maintained for 1 h under the flow of air that was saturated with water vapor at room temperature. It was then cooled to room temperature in air to give the so-called steamed sample.

The calcined, hydrated VAPO-5 was also placed into a glass U-tube with a small glass arm attached. After the H_2 treatment, the reduced VAPO-5 was evacuated at room temperature and was poured into the small attached glass tube, the small attached glass tube was then sealed to keep the sample away from moisture in the air. Prior to the XAS measurement, the sample was removed from the glass tube after breaking the seal, and it was packed into an EXAFS cell and sealed with a Kapton film in an argon-purged dry bag. Although the sample was sealed rapidly in an EXAFS cell with a Kapton film in an inert gas enviroment, this reduced VAPO-5 could still absorb a little bit of moisture from air. So we called it the reduced, partially hydrated VAPO-5.

The X-ray absorption spectra of the VAPO-5 were measured in fluoresence mode at the V K-edge at room temperature. The scanned energy was from 200 eV below the vanadium K absorption edge (~5469.4 eV) to 1100 eV above the edge. Standard V_2O_5 and V_2O_4 powders were used as references, and the signal was detected in the transmission mode in order to perform the energy calibration. To avoid the absorption and scattering effects of air on detection, the in-situ cell was purged with He.

EXAFS Data Analysis. The EXAFS was extracted from the X-ray absorption spectra and was then analyzed by curve fitting using a UWXAFS 3.0 software package[15] and FEFF6[16] program. The EXAFS oscillation in energy space $\chi(E)$ was extracted from experimentally measured absorption coefficient $\mu(E)$ by subtracting an isolated "atom-like" background absorption function μ_0(E), using the relation $\chi(E) = (\mu(E) - \mu_0(E))/\mu_0(E)$. Subsequently, $\chi(E)$ was converted into a k-space function $\chi(k)$, where k is the wavenumber of the ejected photoelectron given by $k = 2\pi(2m_e(E - E_0)/h^2)^{1/2}$, where m_e is the mass of electron. A typical EXAFS function $\chi(k)$ contains some structural parameters such as: N_j, the coordination number of the j-th shell, R_j, the interatomic distance, σ_j^2, the Debye−Waller factor. These useful structural parameters can be obtained by curve-fitting analysis. Both k^2- and k^3-weighted Fourier transformations, without phase shift corrections, were performed on the EXAFS function over the specific k range for each sample. The major contributions were found to result from metal−oxygen interactions with no observable metal−metal contributions at longer distances. The k^3-weighted Fourier transformation in r (distance) space on the EXAFS data and one E_0 value in curve-fittings to examine the EXAFS contributions from the backscattering atoms of low atomic number are presented in the text. The resultant Fourier transforms showed major peaks at ~2.0 Å in r space.

Curve-fitting procedures began with the ab initio calculation of the phase shift and amplitude functions for single-scattering of atom pairs using the FEFF6[16] program. As for the input to

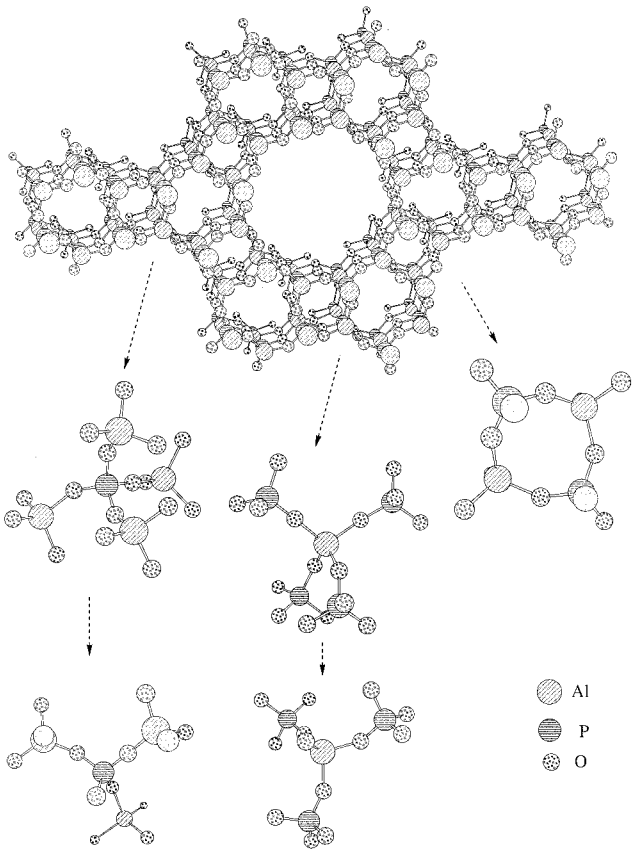

Figure 1. Schematic representation of the generation of molecular models from the framework of the AFI molecular sieve.

FEFF6, we used a known atom cluster from the reference compound V_2O_5 and interatomic distances from the published crystal structure. After calculation, using FEFF6, we obtained theoretical phase-shift and amplitude functions for different atom pairs, including V═O, V−O, and V−V as in V_2O_5. The fitting between the theoretical and the experimental data was made in *r* space within the range of a specific peak. The good-fit parameter, which can also be called the *R* factor,[17] was always found to be below 0.02.

Computational Method

Calculations based on density functional theory[18] were carried out using B3LYP hybrid method involving a three-parameter Becke exchange functional[19] and a Lee−Yang−Parr correlation functional.[20] All of the calculations were performed using a Gaussian-94 program.[21]

Various cluster models were generated, and each represented one of several possible VAPO-5 structures. To generate these models, the CERIUS2 program package[22] was invoked to load the $1 \times 1 \times 1$ unit cell structure of the AFI molecular sieve. First, the cluster of the $2 \times 2 \times 2$ cell was built. Then, the four-ring cluster and the two tetramers in the corners of the four-ring, six-ring, and twelve-ring of this cell were cut, respectively. Finally, the trimers were cut from the tetramers. All of these cuttings are shown in Figure 1. In the sequel, we will substitute either aluminum or phosphorus with vanadium and saturate all of the dangling bonds due to cutting with hydrogen atom.

The first category of the cluster models represents the oxidized forms of VAPO-5. Model Ia1 stands for the case in which the vanadium(V) ion substitutes the phosphorus(V) ion in $AlPO_4$-5. This cluster consists of a $VO_4Al_2(OH)_6^{3-}$ anion.

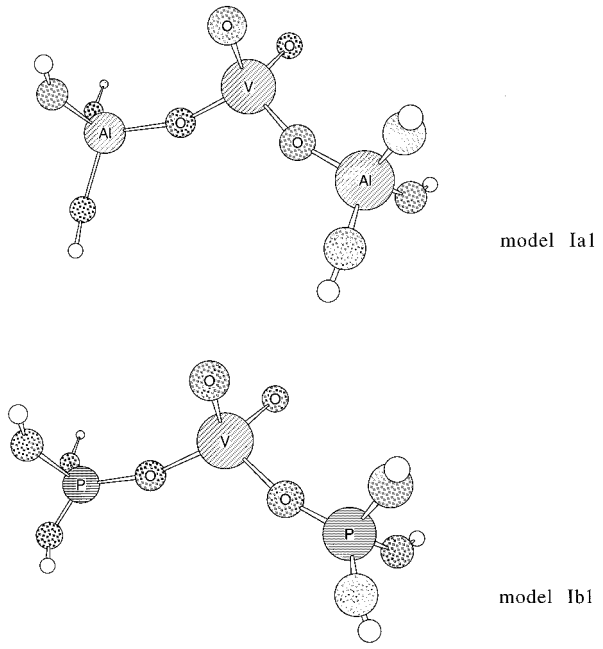

Figure 2. Trimer cluster models of the oxidized form of VAPO-5.

Model Ib1 stands for the case in which the vanadium(V) ion substitutes aluminum(III) ion in $AlPO_4$-5. This cluster consists of a $VO_4P_2(OH)_6^+$ cation. Both models are shown in Figure 2. Model Ia2 stands for the four-ring cluster model of model Ia1. This cluster consists of a $VO_6PAl_2(OH)_6^{2-}$ anion. Model Ib2 stands for the four-ring cluster model of model Ib1. This cluster consists of a $VO_6AlP_2(OH)_6$ molecule. The four-ring models are shown in Figure 3a,b.

The second category represents the reduced forms of VAPO-5. In particular, models IIa1, IIa2, and IIa3 stand for the three possible forms of model Ia1 with four, five, and six oxygen atoms around the vanadium(IV) ion, respectively. These clusters, as indicated in Figure 4, consist of $VO_4Al_2(OH)_6^{4-}$, $VO_5Al_2(OH)_6^{6-}$, and $VO_6Al_2(OH)_6^{8-}$ anions, respectively. Models IIb1, IIb2, and IIb3 are the three possible reduced forms of model Ib1. They are the $VO_4P_2(OH)_6$ molecule, the $VO_5P_2(OH)_6^{2-}$ anion, and the $VO_5P_2(OH)_6^{4-}$ anion, respectively. These models are also shown in Figure 4. The third category, which contains models IIIa and IIIb, represents the original $AlPO_4$-5. As indicated in Figure 5, they are the $PO_4Al_2(OH)_6^{3-}$ and $AlO_4P_2(OH)_6^-$ anion clusters.

Four different Gaussian-type basis sets, denoted as A, B, C, and D, are employed for the B3LYP calculation. The small STO-3G basis set A, is used for the geometry optimization of clusters in the first two categories. For the basis sets B and C, the 6-31G basis set is used to describe the Al and P atoms, and the 6-31G* basis set is used for the O and H atoms. However, for the transition-metal V atom, the (13s10p4d)/[5s4p2d] AKR4 basis set[23] of Rappe, Smedley, and Goddard is used for basis set B. For basis set C, Wachter's 14s9p5d, supplemented by Hay's diffuse 3d function and by 4p functions as in Hood et al. (contracted to 10s8p3d), is used.[24] For basis set D, the 6-31G* basis set is used to describe the O, H, Al, and P atoms, and the AKR4 basis set is used to describe the V atom.

Note that partial geometry optimizations (POPT) are carried out on models of categories 1 and 2 under the following symmetry restrictions: The OTO and TOH angles (where T = Al or P in the TO_4 tetrahedral) and OH bond distances are kept to 109.5°, 150.0°, and 0.0958 nm, respectively. We have also performed the geometry optimization without any constraint

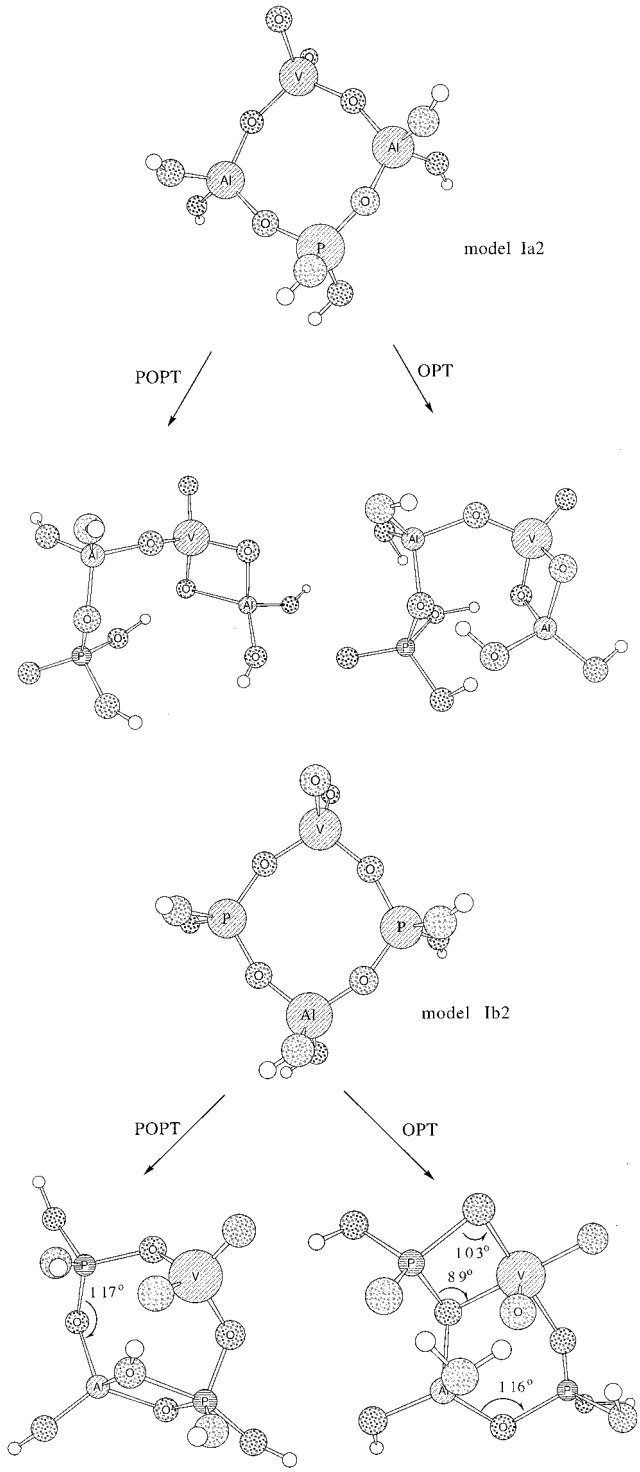

Figure 3. (a). Four-ring cluster model Ia2 of the oxidized form of VAPO-5 and its optimized structures by POPT and OPT calculations. (b). Four-ring cluster model Ib2 of the oxidized form of VAPO-5 and its optimized structures by POPT and OPT calculation.

(OPT)[25] for comparison. For models in category 3, only single-point energy calculations are performed.

Results

V K-edge XANES. The normalized V K-edge XANES spectra of calcined, dehydrated; reduced, dehydrated; and reoxidized VAPO-5 samples are compared with that of the synthesized VAPO-5, V_2O_4, and V_2O_5 references, as shown in Figure 6. Each XANES spectrum consists of a preedge

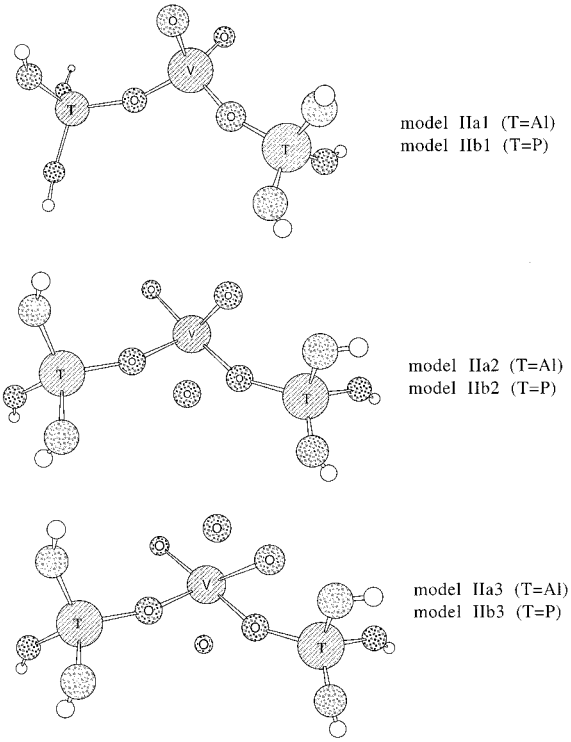

Figure 4. Trimer cluster models of the reduced form of VAPO-5.

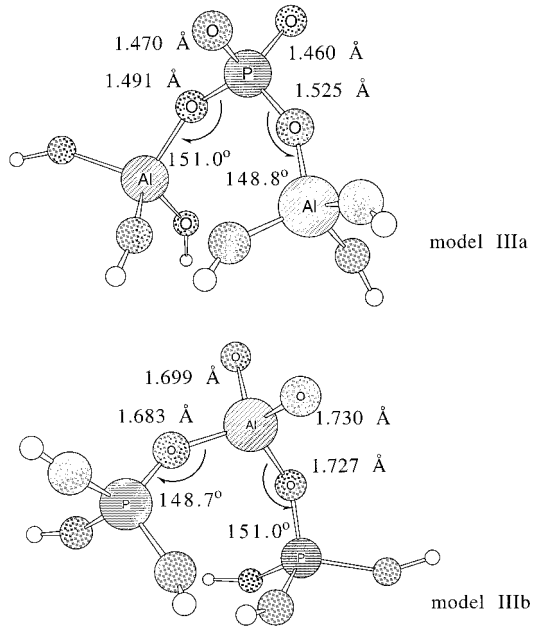

Figure 5. Trimmer cluster models of the original AlPO-5.

absorption peak followed by a rising absorption edge curve. The positions of the preedge peak and the first inflection point of absorption edge curve (threshold energy) are found to be sensitive to the treatment conditions and oxidation states of the vanadium species. Spectra of calcined, dehydrated or reoxidized VAPO-5 are very similar to that of V_2O_5 and are located at about 1 eV (preedge peak) and 4 eV (absorption edge) higher in energy than that of the as-synthesized VAPO-5. The position of preedge peaks and absorption edges of reduced, dehydrated VAPO-5 and reference V_2O_4 are located at slightly lower energy than that of the as-synthesized VAPO-5. This confirms that vanadium ions in the as-synthesized VAPO-5 are mainly in +4 state, and they can be mostly oxidized to a +5 state upon air and oxygen calcination at 500 °C and can be completely reduced

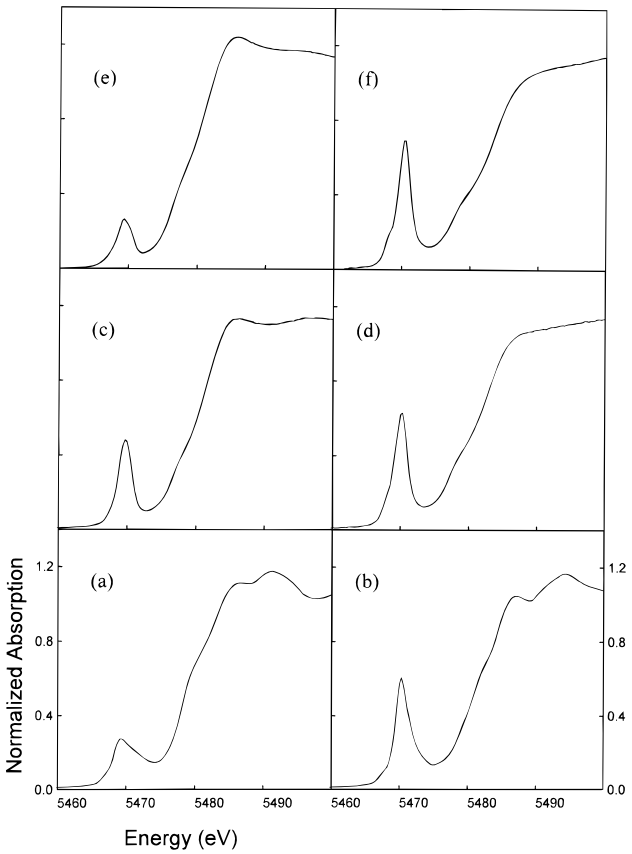

Figure 6. V K-edge XANES spectra of (a) V_2O_4, (b) V_2O_5, (c) synthesized, (d) calcined, dehydrated, (e) reduced, dehydrated, and (f) reoxidized VAPO-5.

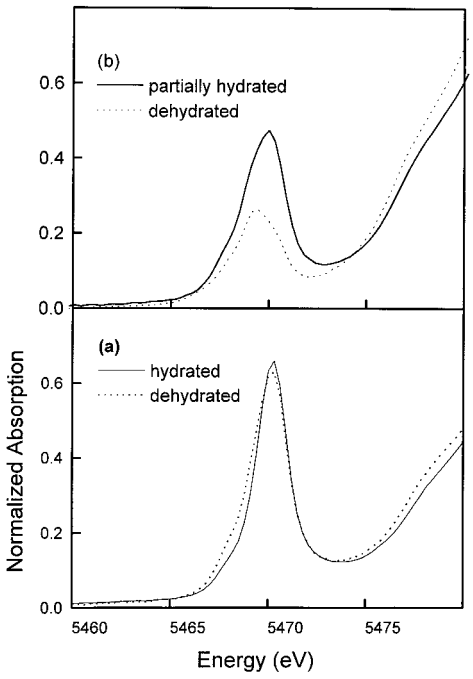

Figure 7. V K-edge XANES spectra of (a) calcined, (b) reduced VAPO-5.

to +4 state after 500 °C hydrogen treatment. The oxidation and reduction between V^{4+} and V^{5+} are reversible.

The intensity variation of preedge peaks across the treatment is noteworthy, as shown in Figures 6 and 7. As for the regular octahedral VO_6 units having a center of inversion, the preedge absorption peak corresponds to 1s → 3d transition, and this is

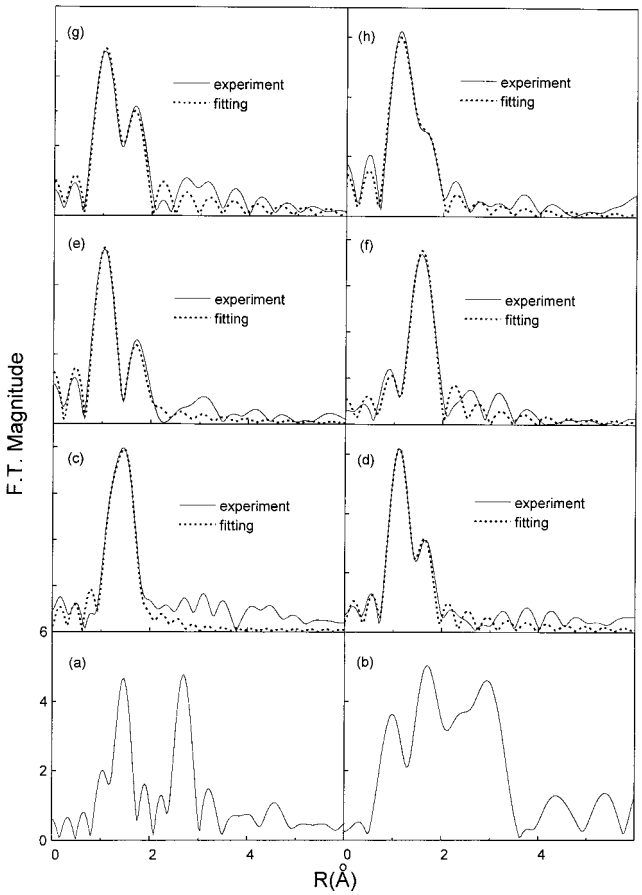

Figure 8. Magnitude of Fourier transform of V K-edge k^3-weighted EXAFS data for (a) V_2O_5, (b) V_2O_4, (c) synthesized, (d) calcined, hydrated, (e) calcined and dehydrated, (f) reduced, dehydrated, (g) reoxidized, and (h) steamed VAPO-5 (note that the phase shifts were not corrected).

quadrupole allowed and dipole forbidden and is expected to be very weak. For cases in which the symmetry of the ligands is lowered from O_h, the inversion center is broken, such as square-pyramidal VO_5 groups of V_2O_5 and tetrahedral VO_4 chains of NH_4VO_3;[26a,b] the preedge absorption becomes intense and is dipole allowed because of a combination of stronger 3d−4p mixing and overlap of the metal 3d orbital with 2p orbitals of ligands. As seen in Figure 6, the coordination symmetry of vanadium(V) oxide units in calcined, dehydrated and reoxidized VAPO-5 seems to be close to square-pyramidal or tetrahedral rather than octahedral. Upon reduction, a drastic decrease in the intensity of preedge peak is observed. The intensity change indicates that the perturbation of coordination symmetry is expected due to the reduction of vanadium(V) ion. The vanadium(IV) oxide units of the reduced, dehydrated VAPO-5 may adopt an octahedral or pseudooctahedral coordination.

The intensity of the preedge peak in reduced VAPO-5 is sensitive to the presence of moisture in the air (Figure 7). After a few minutes of exposure to air at room temperature, an increase in intensity occurs that may be caused by the ligand exchange around vanadium(IV) center. Figure 7 also shows that the preedge-peak feature of both the dehydrated and the hydrated, calcined VAPO-5 are essentially the same. This indicates that the influence of water in the coordination symmetry of vanadium(V) ions is rather small.

V K-edge EXAFS. Figure 8 shows that the EXAFS feature of crystalline V_2O_5 correponds to its structure of the five V−O distances of 1.59, 1.78, 1.88(2), 2.02, and 2.79 Å and the two V−V distances of 3.08 and 3.43 Å.[27] The Fourier transforms

TABLE 1: V K-edge EXAFS Results of All VAPO-5s[a]

sample	shell	R (Å)	CN	V valence[b]	σ^2 (Å^2) × 10^{-3}	ΔE_0 (eV)
synthesized	V−O	1.614(0.018)	1.23(0.22)	3.3	0.3(0.1)	7.42
	V−O	1.992(0.038)	2.32(0.16)		5.7(0.2)	
calcined	V−O	1.612(0.019)	2.16(0.15)	4.9	3.8(0.6)	−1.58
(hydrated)	V−O	1.907(0.027)	1.76(0.16)		5.6(0.6)	
calcined	V−O	1.640(0.025)	2.37(0.13)	5.0	4.2(0.2)	−1.42
(dehydrated)	V−O	1.874(0.092)	1.62(0.29)		1.2(0.1)	
reduced	V−O	1.628(0.025)	1.08(0.00)	4.0	5.4(0.4)	3.67
(dehydrated)	V−O	1.971(0.023)	3.87(0.32)		4.7(0.1)	
reoxided	V−O	1.657(0.011)	2.00(0.00)	4.4	2.2(0.3)	0.50
	V−O	1.838(0.043)	1.60(0.18)		3.8(0.7)	
steamed	V−O	1.606(0.022)	2.10(0.11)	5.2	2.1(0.2)	−6.06
	V−O	1.881(0.024)	2.00(0.00)		5.8(0.1)	
reduced	V−O	1.658(0.015)	1.00(0.00)	2.5	0.3(0.1)	−0.39
(partially hydrated)	V−O	1.944(0.022)	1.75(0.21)		1.3(0.1)	

[a] Values in parentheses are estimated uncertainties. [b] Calculated by the Brown equation.

(FTs) of k^3-weighted EXAFS spectra on VAPO-5 samples consist of peaks contributed from short V−O bonds of approximately 1.60−1.66 Å and long V−O bonds of approximately 1.84−1.99 Å, as shown in Figure 8. No identifiable V−V peak due to V−O−V bonds was observed, an indication that the vanadium oxide units remained in an isolated state on the VAPO-5 surface during redox cycles. Table 1 shows that the coordination number and bond distance for the first-shell atoms around the vanadium atoms on the calcined and hydrated, the calcined and dehydrated, and reoxidized VAPO-5 samples are similar and correspond to tetrahedral VO_4 species with two long V−O bonds and two short V−O bonds. The bond valence (s) and the charge on metal are correlated with their bond length (r). Using an empirical formula of $s = \exp[(r_0 - r)/B]$, where $r_0 = 1.784$ for V^{4+} and 1.803 for V^{5+} and $B = 0.37$, given by Brown et al.,[28] the sum of the bond valences around a V^{5+} center of oxidized VAPO-5 has been calculated to be approximately 4.4−5.2 and is comparable to the expected value of 5.0.

The EXAFS of the reduced, dehydrated sample is attributed to (V═O) O_4, with one short V−O bond of 1.63 Å and four long V−O bonds of 1.97 Å, and to a lower coordination with V−O bonds of 1.78, 1.89, 1.98, 1.99, 2.03, and 2.23 Å as in VO_6 of V_2O_4. However, XRD structure analysis showed that VO_6 units are linked together by sharing corners or edges with the V−V distances of 2.89 and 3.20 Å.[26a,c] The sum of the bond valences for both (V═O)O_4 and VO_6 are 4.0. Moreover, the XANES preedge-peak features of vanadium(IV) oxides in reduced, dehydrated VAPO-5 and V_2O_4 are comparable to the corresponding structure of (V═O)O_4 in a square-pyramidal coordination distorted toward octahedral.

Modeling Calculation. Table 2 shows the calculated V−O bond distances and the total energy of the models in the first category. The results obtained from the small models Ia1 and Ib1 are examined. The V−O bonds initially generated from the unit cell of the AFI molecular sieve are shown in Figure 5, and they were all different, without any apparent regularity before we performed the geometry optimization. However, after geometry optimization, the small basis set A and larger basis sets B, C, and D all generate two short V−O bonds and two longer V−O bonds, and each pair shows the same bond distances for all of the calcined form models. This is consistent with the results obtained from the in-situ XAS.

Notice that the geometry optimization, with and without any symmetry constraint, will give the same qualitative results for all cases. In addition, the results obtained from basis set D are the same as those obtained from basis set B. Thus, the inclusion of the diffuse d function on the P and Al atoms is proven to be unimportant for achieving the convergence in geometry. Similarly, the same is true for the case of vanadium atoms when compared with the results obtained from the basis sets B and C.

TABLE 2: Bond Distances (Å) of V−O Bonds and Total Energies (Hartrees) for the Calcined Form of VAPO-5 Models

cluster	basis set	R_{V-O}	total energy
Ia1	A	1.60, 1.60, 1.71, 1.71[a]	−2158.30
Ia1	A	1.61, 1.61, 1.71, 1.71[b]	−2158.53
Ia1	B	1.65, 1.65, 1.79, 1.80[a]	−2183.91
Ia1	B	1.64, 1.65, 1.79, 1.79[b]	−2184.03
Ia1	C	1.66, 1.66, 1.82, 1.82[a]	−2185.01
Ia1	C	1.66, 1.66, 1.81, 1.81[b]	−2185.13
Ia1	D	1.65, 1.65, 1.79, 1.80[a]	−2183.98
Ia1	D	1.64, 1.64, 1.79, 1.79[b]	−2184.09
Ib1	A	1.56, 1.56, 1.81, 1.81[a]	−2354.33
Ib1	A	1.60, 1.60, 1.75, 1.75[b]	−2354.62
Ib1	B	1.58, 1.58, 1.92, 1.92[a]	−2381.20
Ib1	B	1.59, 1.59, 1.90, 1.90[b]	−2381.31
Ib1	C	1.60, 1.60, 1.93, 1.94[a]	−2382.29
Ib1	C	1.60, 1.60, 1.92, 1.92[b]	−2382.40
Ib1	D	1.59, 1.59, 1.91, 1.91[a]	−2381.49
Ib1	D	1.59, 1.59, 1.90, 1.90[b]	−2381.57
Ia2	A	1.57, 1.65, 1.70, 1.76[a]	−2644.56
Ia2	A	1.57, 1.65, 1.70, 1.76[b]	−2644.83
Ib2	A	1.55, 1.60, 1.75, 1.80[a]	−2742.58
Ib2	A	1.54, 1.67, 1.82, 1.83, 2.18[b]	−2742.87

[a] Results obtained from the POPT method. [b] Results obtained from the OPT method.

As far as the total energy is concerned, the B3LYP/basis B calculations on $AlPO_4$-5 framework of models IIIa and IIIb are −1581.96 and −1680.61 au, respectively. Therefore, from Table 2, the changes in total energies in going from cluster IIIa to Ia and from cluster IIIb to Ib are about −580 and −670 au, respectively, and both processes are thus energetically favorable. As for the bond distance, as indicated in Figure 5, the average P−O bond distance in model IIIa and the average Al−O bond distance in model IIIb are about 1.5 and 1.7 Å, respectively. The V^{5+}−O bond distance in calcined, dehydrated VAPO-5 obtained from the in-situ XAS study is about 1.87 Å. This implies that the substitution of $V^{5+}O_4$ (model Ib) for $Al^{3+}O_4$ (model IIIb) is more favorable. As for the bond angles, we examine the optimized structures of models Ia1 and Ib1 obtained from the POPT method using basis set B. The results indicate that the Al−O−V angles are about 160° in model Ia1 and the P−O−V angles are about 125° in model Ib1. However, the original angles of Al−O−P in the AFI framework are about 150°. Therefore, the bond angles for both models deviate from that of the framework.

The results obtained from the four-ring models using basis set A are further examined. In the case of phosphorus(V) ion being substituted by vanadium(V) ion for model Ia2, one short V−O bond and three bridging V−O−Al bonds are obtained for the case in which both the POPT and the OPT methods are used. Both of the four-ring structures are destroyed as indicated in Figure 3a. In the case of the aluminum(III) ion being substituted by the vanadium (V) ion as in model Ib2, four different V−O bonds are obtained for cases in which the POPT method is used; and one short and four long V−O bonds are obtained for instances in which the OPT method is used. Both of the optimized structures are rearranged and the P−O−Al angles were reduced to about 110°, as shown in Figure 3b, of which, the structures consist of edge-shared phosphorus sites that are the least likely structures for zeolite frameworks. In

TABLE 3: Atomic Net Charges on T (Q_v, Q_T in E-) and O Atoms that Connected to the Central Atom Where T = V, Al or P of $AlPO_4$-5 Models and Calcined VAPO-5

cluster	Q_V	Q_{Al}	Q_P	Q_O
Ia1[a]	0.25	0.97, 0.98		0.51, −0.51, −0.54, −0.53
III[a]		1.42, 1.42	1.71	−0.94, −0.95, −1.01, −1.03
Ib1[a]	0.55		1.38, 1.38	−0.34, −0.38, −0.38, −0.38
III[b]		1.33	1.76, 1.77	−0.71, −0.71, −0.92, −0.96

[a] Results obtained from the POPT method.

TABLE 4: Bond Distances (Å) of V−O Bonds and Total Energies (Hartrees) for the Reduced Form of VAPO-5 Models

cluster	R_{V-O}/Å	total energy
IIa1	1.61, 1.61, 1.68, 1.76[a]	−2157.53
IIb1	1.54, 1.74, 1.76, 1.85, 2.32[a]	−2354.39
IIb1	1.54, 1.75, 1.80, 1.81, 2.04[b]	−2354.73
IIb2	1.56, 1.75, 1.81, 1.89, 2.17, 2.28[a]	−2428.15
IIb2	1.56, 1.73, 1.79, 1.80, 2.03[b]	−2428.59

[a] Results obtained from the POPT method. [b] Results obtained from the OPT method.

addition, the optimized structures of the vanadium ion for models Ia2 and Ib2 are inconsistent with the in-situ XAS study. Hence, the vanadium can neither substitute the framework aluminum nor the phosphorus in the four-ring. Furthermore, it can be seen that every phosphorus or aluminum atom of the AFI zeolite is in the corner of a four-ring. Therefore, the conjecture of substitution by vanadium is not plausible in the AFI framework.

Table 3 gives the calculated atomic net charges on T (where T = V, Al, or P) and O atoms when basis set A is used. The net charges of P in model IIIa, Al in model IIIb, V in model Ia1, and V in model Ib1 are 1.71, 1.33, 0.25, and 0.55 e−s, respectively following Mulliken population analysis. The net charges of vanadium are further noticed to be very different from both aluminum and phosphorus. The net charges of the oxygen atoms that were connected to the vanadium were also different from those connected to that of either aluminum or phosphorus. These results also support the fact that vanadium-(V) ions may not substitute aluminum or phosphorus ions in AFI framework.

Table 4 shows the calculated V−O bond distances and total energies of the reduced VAPO-5 of models (IIa1, IIa2, and IIa3) when basis set A is used. The results obtained from the POPT method are examined. First, in the case of phosphorus(V) being substituted by vanadium(IV), V−O distances of 1.61, 1.61, 1.68, and 1.76 Å are obtained for model IIa1. For models IIa2 and IIa3, the optimized structure cannot be obtained, regardless of how the initial condition of the fifth and sixth O atoms are set. One or two O atoms, or the −OH group, tend to move farther away from the central V atom during the optimization process. One short V−O bond and four long V−O bonds of the reduced form of VAPO-5 are observed in the in-situ XAS study. Therefore, the vanadium(IV) oxide cannot bond only to two aluminum atoms in the framework. In model IIb1, in which aluminum is substituted by vanadium, the four V−O distances of 1.54, 1.74, 1.76, and 1.85 Å are obtained. The optimized structure is shown in Figure 9. In this figure, the next nearest oxygen atom to vanadium is 2.32 Å and one phosphorus is in a rare 5-fold coordination. This indicates that more than two TO_4 (T = Al or P) units might be required to bond to one vanadium(IV) oxide; the five oxygen atoms around vanadium thus form a square pyramidal structure. For model IIb2, the calculation depends on the initial condition of the fifth O atom. According to Table 4, the structure of the vanadium of optimized

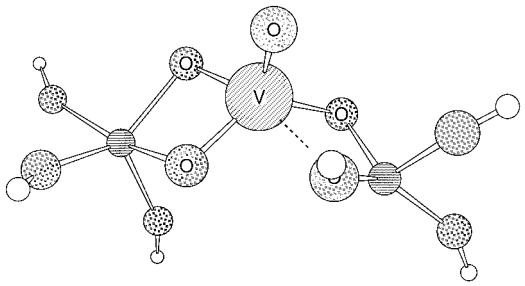

Figure 9. The optimized structure of model IIb1.

model IIb2 is close to that of a distorted octahedron. As for the case of model IIa3, the optimized structure of model IIb3 has never been found.

The results obtained from the OPT method were then examined. For models IIb1 and IIb2, the optimized structures of vanadium are close to square pyramidal. According to Tables 2 and 4, the agreement among the results obtained from the POPT method and the OPT method depends on the models that are employed.

So far, the results indicate that the vanadium(IV) oxide cannot bond to just two Al's, yet it is able to bond to two P's in the framework. Furthermore, we have performed geometry optimization on the reduced form of the four-ring model Ib2 with five oxygen atoms around the vanadium(IV) ion using basis set A. This cluster consists of a $VO_7AlP_2(OH)_6^{3-}$ anion. The structure came apart during the optimization process, and one P−O−Al bridge was destroyed. Either two −OH groups or one −OH group will leave the phosphorus ions, which depends on whether the POPT or OPT method is used. Again, the results indicate that vanadium cannot isomorphously substitute for the aluminum in the framework.

Discussion

The results in models Ia2 and Ib2 (refer to model calculation) have indicated that the substitutions of either aluminum or phosphorus by vanadium are, in general, implausible. In addition, the Mulliken population analysis has indicated that the net charge of vanadium is very different from that of both aluminum and phosphorus in the framework. As for models Ia1 and Ib1, the results in Table 2 have indicated that the optimized structures from both models are consistent with the in-situ XAS study. For instance, according to our models, Ia1 and Ib1, the average distances of four V−O bonds are 1.63, 1.63, 1.87, and 1.87 Å, respectively, for cases in which basis set C is used. The corresponding values of in-situ XAS study are 1.64, 1.64, 1.87, and 1.87 Å, respectively. They match on a one-to-one basis. One reasonable explanation for this fact is that vanadium oxide may dock to the framework of AFI.

With regard to the pores, there are six four-rings, four six-rings, and two twelve-rings per unit cell of AFI. The nearest P−P or Al−Al distances are about 4.0, 5.0, and 5.6 Å for the four-ring, six-ring, and twelve-ring, respectively. Our calculated Al−Al distance for model Ia1 and P−P distance for model Ib1 are about 5.9 Å. Therefore, pores from the four-rings and six-rings are too small to allow bond formation. The most probable pore should be the twelve-ringed one. Hence, we propose that the docking $V^{5+}O_4$ of model Ia1 or Ib1 is to the twelve-ring. The illustration is provided in Figure 10a,b.

Both XAS and model calculation indicate that the structure for surface vanadium(V) oxide units in calcined or oxidized VAPO-5 is a tetrahedral $V^{5+}O_4$ and consists of two short V−O bonds and two long V−O bonds instead of the mono-oxo

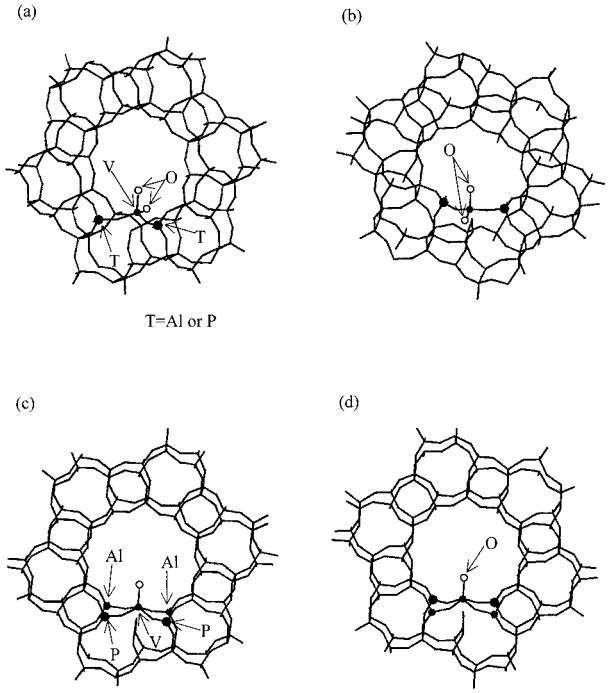

Figure 10. Schemes of V^{4+} and V^{5+} cations docking to the twelve-ring; (a) the front view and (b) the back view of $V^{5+}O_4$ (model Ia1 or Ib1), (c) the front view and (d) the back view of $V^{4+}O_5$ grafted in the AFI molecular sieve.

vanadyl group of a $(V{=}O)^{3+}$ unit with the three bridging V−O proposed previously.[2,6] The two short bonds can be considered as di-oxo double bonds, similar to that of chain vanadates of NH_4VO_4, whereas the bridging V−O−T bond may allow the anchoring of $V^{5+}O_4$ units to TO_4(T = Al or P) framework sites through oxygen corner sharing.

For cases in which water vapor is present, di-oxo vanadates present an axially asymmetric ^{51}V NMR powder pattern[5] that corresponds to a square pyramidal structure, which, in turn, is attributed to the additional long-distance coordination of water molecule to the hydrated VO_4 units. In view of the disorder of $V{\cdots}OH_2$ interaction, the H_2O contribution cannot be detected from the EXAFS data and has not been included in the model calculation. The structure of vanadium(V) oxides on other inorganic oxides and molecular sieves have been examined extensively. Structures of highly dispersed V_2O_5 on Al_2O_3 and TiO_2 have been proposed in the literature as either di-oxo vanadates or mono-oxo vanadyl groups.[29−32] However, mono-oxo vanadyl groups were usually considered to be the surface vanadium(V) oxide units supported on SiO_2 and silicate molecular sieves.[33−36] After water adsorption, isolated $(V{=}O)$-$(O_f)_3$ units of calcined and hydrophilic V−MCM-41 molecular sieves were observed to be linked together through surface Si−OH groups, based on in-situ XANES/EXAFS analysis.[35] Upon hydration, the absence of V−O−V formation on calcined VAPO-5 revealed that monomeric V^{5+} oxide species are more stable on a microporous aluminophosphate framework than on a mesoporous silicate framework, and they retain their locations during hydration and dehydration. Water molecules may be coordinated to vanadium(V) centers without breaking the bridging V−O−T bonds and thus cause the shift in symmetry of V^{5+} ions from tetrahedral to square pyramidal.

Raman spectroscopic studies[36] showed that the effect of water vapor on the structures of surface V^{5+} species is more pronounced on Al_2O_3 support than on hydrophobic SiO_2 support, and the terminal V=O and bridging V−O−V bond can undergo

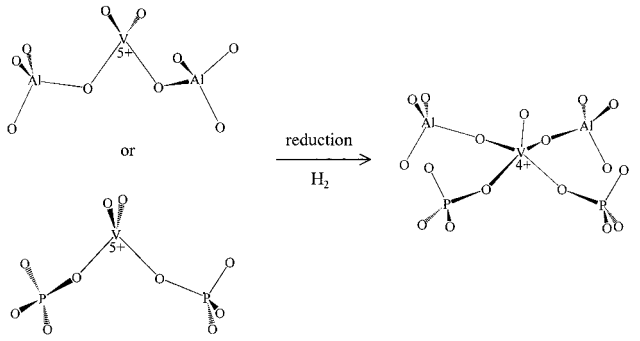

Figure 11. The proposed scheme of reduction of V^{5+} species to V^{4+} species on the AFI framework.

oxygen exchange with water vapor. In vanadium phosphates, their chain and layer structures are composed of shared corners of oxygen through one V=O bond of di- and mono-oxo vanadate groups and one or more V−O bonds of a vanadate unit as identified by XRD structural analysis.[37−39]

It is conceivable that in VAPO-5, the reduction of V^{5+} to V^{4+} takes place through the interaction between the vanadium atom and either the surface hydroxyl group or the framework oxygen atom. The reduction can be described as a hydrogen molecule that reacts with the oxygen atom of a V=O bond of the di-oxo $V^{5+}O_4$ unit to form a removable water molecule accompanied by a ligand vacancy on vanadium species, two nearby O_f's from separated framework TO_4 sites may then attach to vanadium to generate a $(V^{4+}{=}O)(O_f)_4$ unit. The EXAFS and XANES results indicate that surface V^{4+} species may exist as $V{=}O^{2+}$ mono-oxo-vanadyl ions coordinated to the framework surface through either two oxygens in partially hydrated state or four oxygens in dehydrated state, and they adopt pyramidal or distorted octahedral, rather than tetrahedral, coordination.

On the basis of such findings, the plausible structures of V^{4+} and V^{5+} species in oxidation−reduction process are presented in Figures 10 and 11. The compositions of the oxidized vanadia-phosphate pair and the reduced vanadia-aluminophosphate cluster in dehydrated AFI can be described as $[VO_2O_{2/2}{\cdot}PO_{4/2}]$ and $[VOO_{4/2}{\cdot}Al_{1/2}P_{1/2}O_{4/2}]$, respectively, with each bridging oxygen shared by one V atom and one P or Al atom. However, V seems to be bonded to two P sites on the same twelve-ring. Upon reduction, V ions possess two more V−O bridging bonds to attach to two Al sites on the next twelve-ring. This can explain the results of composition and EPR investigations reported in the literature.[2−4,6−8] If every four twelve-ring's contains one vanadium ion, the calculated content of vanadium in VAPO-5 is 1.7 wt %, which matches very well with the experimental findings. The content of vanadium in as-synthesized VAPO-5 is 1.8 wt %. However, the bonding of vanadium(IV) oxide to the twelve-ring is worth further investigation and will appear in the sequel.

The variation of coordination geometry derived from the interaction between water and vanadium oxide units on calcined and reduced VAPO-5 is quite interesting. This variation may correlate with the unique catalytic properties of transition-metal incorporated molecular sieves that show strong dependence on the specific coordination chemistry of metal ions, as well as on the interaction between adsorbate and metal ions.

Acknowledgment. This work was supported by the National Science Council of Republic of China

References and Notes

(1) Concepcion, P.; Corma, A.; Lopez Nieto, J. M.; Perez-Paricnte, J. *Appl. Catal., A* **1996**, *143*, 17.

(2) Rigutto, M. S.; Bekkum, H. V. *J. Mol. Catal.* **1993**, *81*, 77.
(3) Jhung, S. H.; Uh, Y. S.; Chon, H. *Appl. Catal.* **1990**, *62*, 61.
(4) Montes, C.; Davis, M. E.; Murray, B.; Narayona, M. *J. Phys. Chem.* **1990**, *94*, 6431.
(5) Chao, K. J.; Wu, C. N.; Chang, H.; Lee, L. J.; Hu, S. F. *J. Phys. Chem. B.* **1997**, *101*, 6341.
(6) Prakash, A. M.; Kevan, L. *J. Phys. Chem. B* **1999**, *103*, 2214.
(7) Weckhuysen, B. M.; Vannijvel, I. P.; Schoonheydt, R. A. *Zeolites* **1995**, *15*, 482.
(8) Lohse, U.; Buckner, A.; Kintscher, K.; Parlitz, B.; Schreier, E. *J. Chem. Soc. Faraday Trans.* **1995**, *91*, 1173.
(9) Chao, K. J.; Wei, A. C.; Wu, H. C.; Lee, J. F. *Catal. Today* **1999**, *49*, 277.
(10) Blasco, T.; Concepcion, P.; Lopez Nieto, J. M.; Pere-Pariente, J. *J. Catal.* **1995**, *152*, 1.
(11) Bellussi, G.; Rigutto, M. S. *Surf. Sci. Catal.* **1994**, *85*, 117.
(12) The EXAFS Co., HC 74 BOX 236, Eagle Valley Road, Pioche, NV 89043.
(13) Lytle, F. W.; Greegor, R. B.; Marques, E. C.; Sandstrom, D. R.; Via, G. H.; Sinfelt, J. H. *J. Catal.* **1985**, *95*, 546.
(14) Lytle, F. W.; Greegor, R. B.; Marques, E. C. Proceedings of the Ninth International Congress on Catalysis; M. J. Phillips, M. Ternan, Eds.;The Chemical Institute of Canada: Otlawa, 1988, 5, pp 54.
(15) Stern, E. A.; Newville, M.; Yacoby, Y.; Haskel, D. *Physica B* **1995**, *208*, 117.
(16) Rehr, J. J.; Mustre de Leno, J.; Zabinsky, S. I.; Alberts, R. C. *J. Am. Chem. Soc.* **1991**, *113*, 5135.
(17) Gear, C. W. *Numerical Initial Value Problems in Ordinary Ditterential Equations*; Prentice Hall: New York, 1971.
(18) Kohn, W.; Sham, L. J. *Phys. Rev. A* **1965**, *140*, 1133.
(19) Becke, A. D. *J. Chem. Phys.* **1993**, *98*, 5648.
(20) Lee, C.; Yang, W.; Parr, R. G. *Phys. Rev. B* **1988**, *37*, 785.
(21) Gaussian 94 (Revision E.2): Frisch, M. J.; Trucks, G. W.; Schlegel, H. B.; Gill, P. M. W.; Johnson, B. G.; Robb, M. A.; Cheeseman, J. R.; Keith, T. A.; Petersson, G. A.; Montgomery, J. A.; Raghavachari, K.; Al-Laham, M. A.; Zakrzewski, V. G.; Ortiz, J. V.; Foresman, J. B.; Cioslowski, J.; Stefanov, B. B.; Nanayakkara, A.; Challacombe, M.; Peng, C. Y.; Ayala, P. Y.; Chen, W.; Wong, M. W.; Andres, J. L.; Replogle, E. S.; Gomperts, R.; Martin, R. L.; Fox, D. J.; Binkley, J. S.; Defrees, D. J.; Baker, J.; Stewart, J. P.; Head-Gordon, M.; Gonzalez, C.; Pople, J. A. Gaussian Inc.: Pittsburgh, PA, 1995.
(22) CERIUS2 products are commercially available from Molecular Simulation Inc., San Diego, CA.
(23) Rappe, A. K.; Smedley, T. A.; Goddared, W. A., III *J. Phys. Chem.* **1981**, *85*, 2607.
(24) (a) Wachters, A. J. H. *J. Chem. Phys.* **1970**, *52*, 1033. (b) HAY, P. J. *J. Chem. Phys.* **1977**, *66*, 4377. (c) Hood, D. A.; Pitzer, R. M.; Schaefer, H. F., III *J. Chem. Phys.* **1979**, *71(2)*, 705.
(25) The total energies of the optimized geometries have been checked to ensure that they are indeed minima and not other types of stationary points.
(26) (a) Wong, J.; Lytle, F. W.; Maylotte, D. H.; Messmer, R. P. *Phys. Rev. B* **1984**, *30*, 5596−5610. (b) Yoshida, S.; Tanaka, T.; Hanada, T.; Hiraiwa, T.; Kanai, H.; Funabiki, T. *Catal. Lett.* **1992**, *12*, 277−286. (c) Oka, Y.; Yao, T.; Yamamoto, N. *J. Solid State Chem.* **1990**, *86*, 116.
(27) Enjalbert, R.; Galy, J. *Acta Crystallogr.* **1986**, *C42*, 1467.
(28) Brown, I. D.; Altermatt, D. *Acta Crystallogr*. **1985**, *B41*, 244.
(29) Went, G. T.; Oyama, S. T.; Bell, A. T. *J. Phys. Chem.* **1990**, *94*, 4240.
(30) Hardcastle, F. D.; Wachs, I. E. *J. Phys. Chem.* **1991**, *95*, 5031.
(31) Das, N.; Eckert, H.; Hu, H.; Wachs, E.; Walzei, J. F.; Feher, F. J. *J. Phys. Chem.* **1993**, *97*, 8240.
(32) Sen, T.; Ramaswamy, V.; Ganapathy, S.; Rajamohanan, P. R.; Sivasanker, S. *J. Phys. Chem.* **1996**, *100*, 3809.
(33) Kornatowski, J.; Wichterlova, B.; Jirkovsky, J.; Loffer, E.; Pilz, W. *J. Chem. Soc., Faraday Trans.* **1996**, *92*, 1067.
(34) Centi, G.; Perathoner, S.; Trifiro, F.; Aboukais, A.; Aissi, C. F.; Guelfon, M. *J. Phys. Chem*. **1992**, *96*, 2617.
(35) Wei, A. C.; Wu, H. C.; Lee, J. F.; Chao, K. J. Proceedings of 12th IZA, M. M. J. Treacy, B. K. Marcus, M. E. Bisher, J. B. Higgins, Eds.; Materials Research Society: Pennsylvania, 1998, 857.
(36) Jehng, J. M.; Deo, G.; Weckhuysen, B. M.; Wecks, I. E. *J. Mol. Catal.* **1996**, *110*, 41.
(37) Korthuis, V. C.; Hoffmann, R. D.; Huang, J. F.; Sleight, A. W. *Chem. Mater.* **1993**, *5*, 206.
(38) Kang, H. Y.; Wang, S. L.; Tsai, P. P.; Lii, K. H. *J. Chem. Soc., Dalton Trans.* **1993**, *32*, 5.
(39) Tietze, H. R. *Aust. J. Chem.* **1981**, *34*, 2035.